The effect of oxygen isotope substitution on the phase diagram of nearly half-doped $R_{1-x}Sr_xMnO_3$ manganites (R = Sm, NdTb, NdEu)

2005 J. Phys.: Condens. Matter 17 1975

(http://iopscience.iop.org/0953-8984/17/12/019)

INSTITUTE OF PHYSICS PUBLISHING JOURNAL OF PHYSICS: CONDENSED MATTER

J. Phys.: Condens. Matter **17** (2005) 1975–1984 doi:10.1088/0953-8984/17/12/019

The effect of oxygen isotope substitution on the phase diagram of nearly half-doped $R_{1-x}Sr_xMnO_3$ manganites (R = Sm, NdTb, NdEu)

N A Babushkina[1], E A Chistotina[1], I A Bobrikov[2], A M Balagurov[2], V Yu Pomjakushin[3], A I Kurbakov[4], V A Trunov[4], O Yu Gorbenko[5], A R Kaul[5] and K I Kugel[6]

[1] Russian Research Centre, 'Kurchatov Institute', Kurchatov Square 1, Moscow, 123182, Russia
[2] Frank Laboratory of Neutron Physics, Joint Institute for Nuclear Research, Dubna, Moscow region, 141980, Russia
[3] Laboratory for Neutron Scattering, ETH Zurich and Paul Scherrer Institute, CH-5232, Villigen PSI, Switzerland
[4] Saint Petersburg Institute of Nuclear Physics, Russian Academy of Sciences, Gatchina, Leningrad region, 188300, Russia
[5] Department of Chemistry, Moscow State University, Vorobievy Gory, Moscow 119899, Russia
[6] Institute for Theoretical and Applied Electrodynamics, Russian Academy of Sciences, Izhorskaya street 13/19, Moscow, 125412, Russia

E-mail: babushkina@imp.kiae.ru

Received 24 November 2004, in final form 11 February 2005
Published 11 March 2005
Online at stacks.iop.org/JPhysCM/17/1975

Abstract

The effect of $^{16}O \rightarrow {}^{18}O$ isotope substitution on the electrical resistance, magnetic susceptibility and neutron diffraction patterns of nearly half-doped $R_{1-x}Sr_xMnO_3$ manganites was studied for ceramic samples with R = Sm ($x = 0.425$–0.525), Nd/Tb ($x = 0.45$) and Nd/Eu ($x = 0.45$). In Nd/Tb and Nd/Eu manganites, the composition was chosen to yield the same mean ionic radius as in the Sm compound, but the samples differed in the cation disorder parameter σ. The oxygen isotope substitution leads to fundamental changes in the phase diagram of the manganites studied, favouring enhanced inhomogeneity, stabilizing the insulating antiferromagnetic (AFM) state and even causing a metal–insulator transition (MIT). The MIT induced by the oxygen isotope substitution was found here for the first time in manganites with A-type AFM; earlier this unusual phenomenon was observed only for compounds with the CE-type AFM structure. This suggests that such a MIT is closely related to the ferro–AFM crossover independently on the specific nature of the AFM phase and related orbital order.

1. Introduction

Recent experimental and theoretical studies clearly demonstrate the importance of the existence of various-scale phase separation in the perovskite manganites $R_{1-x}A_xMnO_3$, where R is a rare earth element and A is an alkaline earth element. Both microscopic (∼15–20 Å) and mesoscopic (∼500–2000 Å) phase separation have been experimentally revealed (see, for instance, [1–3] and references therein) and theoretically analysed [4–6].

The mesoscopic phase separation, which at low temperatures often manifests itself in the form of an incoherent mixture of ferromagnetic (FM) metallic and antiferromagnetic (AFM) insulating domains, is most clearly pronounced near the crossover between metallic and insulating states, where their ground state energies are close to each other. A good example of such behaviour is provided by the $(La_{1-y}Pr_y)_{0.7}Ca_{0.3}MnO_3$ compound with $y = 0.75$, where, as a consequence of the phase separated state, the giant oxygen isotope effect (a metal–insulator transition induced by $^{16}O \rightarrow {}^{18}O$ substitution) is seen [7]. The neutron diffraction experiments on this compound revealed that the changes in electrical transport properties correlate with the changes in magnetic structure: upon temperature lowering the sample with ^{16}O undergoes successive antiferromagnetic (with the CE-type ordering, $T_N = 145$ K) and ferromagnetic ($T_C = 115$ K) transitions, resulting in an incoherent mixture of ferromagnetic and antiferromagnetic regions, while in the sample with ^{18}O an homogeneous AFM structure of CE type ($T_N = 145$ K) is found [8].

Extending these investigations to other systems, we studied the effect of oxygen isotope substitution on the transport properties and magnetic structure of $Sm_{1-x}Sr_xMnO_3$ manganites with x close to 0.5, i.e. in the region where the hole doping is changing to the electron one. Such a crossover could also favour the phase separation. Indeed, for $Nd_{1-x}Sr_xMnO_3$ it was found [9, 10] that near $x = 0.5$ (at the boundary between ferromagnetic–metallic (FM–M) and antiferromagnetic (A-type)–metallic (AFM_A–M) phases) there appears also a antiferromagnetic (CE-type) charge ordered insulating (AFM_{CE}–CO–I) phase.

The average A-type cation radius, $\langle r_A \rangle$, in the $Sm_{1-x}Sr_xMnO_3$ (SSM-x hereafter) compound is only slightly smaller than in the Nd–Sr system and one may expect similar behaviour from the viewpoint of phase coexistence. The first phase diagram for SSM perovskite constructed using data on electrical resistance, magnetization and electron diffraction was reported in [11]. It exhibits a broad region of ferromagnetic metallic state at $0.3 < x \leqslant 0.52$, the existence of which was related in [11] to the rather large $\langle r_A \rangle$ in the Sm–Sr system. The neutron powder diffraction study of $Sm_{0.6}Sr_{0.4}MnO_3$ provided an opportunity to reveal [12, 13] the coexistence of FM and AFM ordering at low temperatures and the unusual large coherent Jahn–Teller distortions of the oxygen octahedra, which remain even in the FM–M state.

In [14], a pronounced oxygen isotope effect was reported for Sm–Sr compositions close to $x = 0.5$ and even a transition to the insulating state (at $x = 0.475$ and 0.5) was observed. To achieve a better understanding of the high sensitivity of all physical properties of SSM-x to small changes in the composition, we also performed neutron diffraction studies of $Sm_{1-x}Sr_xMnO_3$ compounds [15]. In the present paper, we review the results obtained earlier and report new important data on structural and magnetic isotope effects in $R_{1-x}Sr_xMnO_3$ with $x = 0.425, 0.450, 0.475, 0.500$ and 0.525 for R = Sm; and with $x = 0.450$ for R = (Nd/Tb) and (Nd/Eu) [14–16]. The relative Nd/Tb and Nd/Eu content was matched to make the average ionic radius $\langle r_A \rangle$ equal to $\langle r_A \rangle$ in SSM-x.

2. Experimental details

Ceramic samples of $R_{1-x}Sr_xMnO_3$ were prepared by the so-called 'paper synthesis' technique. An aqueous solution of a mixture of metal nitrates in the required ratios was deposited on an

ash-free paper filter, which was dried (120 °C) and then burnt. The synthesis was performed in air at 700 °C for 2 h. Finally, the pressed pellets were annealed at 1200 °C for 12 h.

The oxygen isotope exchange $^{16}O \rightarrow {}^{18}O$ was performed at $T = 950$ °C at pressure $p = 1$ bar for 500 h using the method reported in [7]. Two samples were treated simultaneously: one was heated in natural $^{16}O_2$; the other one was heated in $^{18}O_2$ (92% enrichment).

The resistivity of the samples was measured by the conventional four-probe technique in the temperature range from 4.2 to 300 K. The measurements of the real part of the ac magnetic susceptibility $\chi(T)$ were performed in an ac magnetic field with frequency 667 Hz and an amplitude of about 0.4 Oe. Neutron diffraction experiments were performed on several instruments: G4.1 and G4.2 at Laboratoire Leon Brillouin (Saclay, France), DMC at the Paul Scherrer Institute (Villigen, Switzerland) and HRFD at the Frank Laboratory of Neutron Physics (Dubna, Russia). For samples with Sm, we used the ^{152}Sm isotope, which allowed us to significantly reduce the absorption coefficient.

It is evident that the necessary condition for correct comparison of the results obtained on the samples with different oxygen isotopes is their identity from the point of view of oxygen content. Our x-ray diffraction studies for the Sm–Sr system demonstrated the structural identity of the samples with different isotopes. There were no significant changes in the lattice parameters even after annealing the samples in argon. This is a good indication that the stoichiometry of the samples is not affected by the oxygen isotope substitution.

Our previous neutron diffraction studies of the LPCM-y system (see details in [8, 17]) also showed that the procedure, which is used for sample preparation, maintains the oxygen stoichiometry with quite high precision. For instance, the analysis of the lattice parameters as a function of the oxygen content demonstrated that the difference in these parameters for the samples with ^{16}O and ^{18}O isotopes is about or less than ± 0.002.

3. Macroscopic properties

In figures 1(a) and (b), we present the temperature dependence of the electrical resistivity measured for all samples under study, with both ^{16}O and ^{18}O isotopes. It turned out that the samples annealed in ^{16}O pass to the metallic state at all values of x, except $x = 0.525$, whereas the ^{18}O-substituted samples become metallic only for two compositions ($x = 0.425$ and 0.450); the other samples are insulators over the whole temperature range. Therefore, for compositions with $x = 0.475$ and 0.500, the oxygen isotope substitution leads to the transformation from the metallic to the insulating state at low temperatures (see the inset to figure 1(a)). A relatively low magnetic field ($H = 1$ T) transforms these samples with ^{18}O again to the metallic state (see the inset to figure 1(b)).

The temperature dependence of the magnetic susceptibility χ for the samples with ^{16}O and ^{18}O is shown in figures 2(a) and (b), respectively. For samples with ^{16}O and $x = 0.425$, 0.450 and 0.475, $\chi(T)$ behaves in a similar manner (as far as the magnitudes of χ and T_C are concerned). The Curie temperature T_C was determined as a point corresponding to the maximum value of $d\chi(T)/dT$. For $x = 0.500$, the χ value drops drastically and shifts toward lower temperatures. This is a signature of the decreasing contribution of the FM phase. For the composition with $x = 0.525$ the susceptibility becomes very small and the ferromagnetism almost disappears.

The samples with ^{18}O are characterized by a wider temperature hysteresis as compared to the similar compositions with ^{16}O. The measurements of magnetic susceptibility for the samples with ^{18}O demonstrate that the content of FM phase strongly decreases with the growth of the Sr concentration. Eventually, the FM phase content becomes insufficient for the formation of the percolation paths over the FM metallic regions and the samples become

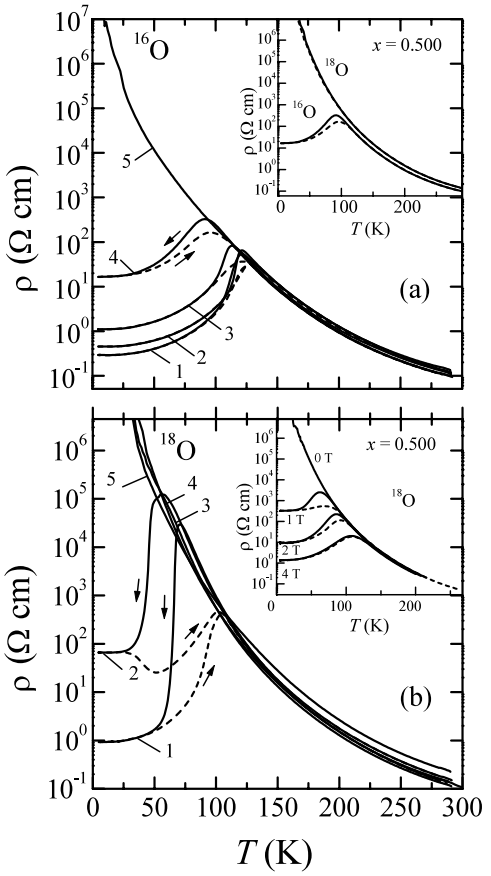

Figure 1. Temperature dependence of the electrical resistivity for $Sm_{1-x}Sr_xMnO_3$ samples with $x = 0.425$ (1), 0.450 (2), 0.475 (3), 0.500 (4) and 0.525 (5). The results for samples with ^{16}O and ^{18}O are presented in panels (a) and (b), respectively. Solid and dashed curves correspond to cooling and heating, respectively. The inset in panel (a) illustrates the metal–insulator transition induced by the oxygen isotope substitution for the samples with $x = 0.500$. The inset in panel (b) shows the magnetic field dependence of the $\rho(T)$ curves for the $x = 0.500$ sample with ^{18}O.

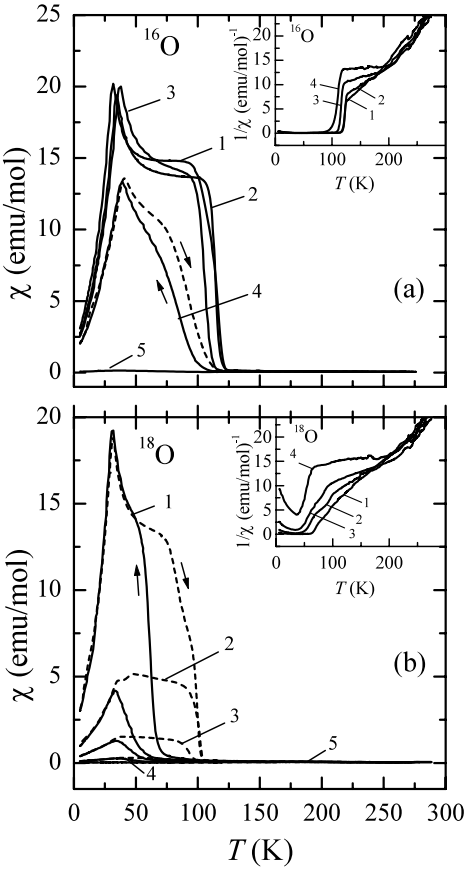

Figure 2. Temperature dependence of the ac magnetic susceptibility for $Sm_{1-x}Sr_xMnO_3$ with $x = 0.425$ (1), 0.450 (2), 0.475 (3), 0.500 (4) and 0.525 (5). The behaviour of the inverse susceptibility is illustrated in the insets. The results for samples with ^{16}O and ^{18}O are presented in panels (a) and (b), respectively. Solid and dashed curves correspond to cooling and heating, respectively.

insulating. This is the case for $x = 0.475$ and 0.500, according to the $\rho(T)$ data. As a result, we see that the $^{16}O \rightarrow {}^{18}O$ isotope substitution in $Sm_{1-x}Sr_xMnO_3$ causes significant changes in the phase diagram at the crossover between the FM–M and AFM–I regions.

4. Neutron diffraction studies

The implementation of a neutron diffraction to the study of the crystal and magnetic structure of Sm-containing manganites is quite problematic due to the very large neutron absorption in natural samarium. However, the situation can be substantially improved by using samples with the ^{152}Sm or ^{154}Sm isotopes for neutron diffraction experiments. The first neutron

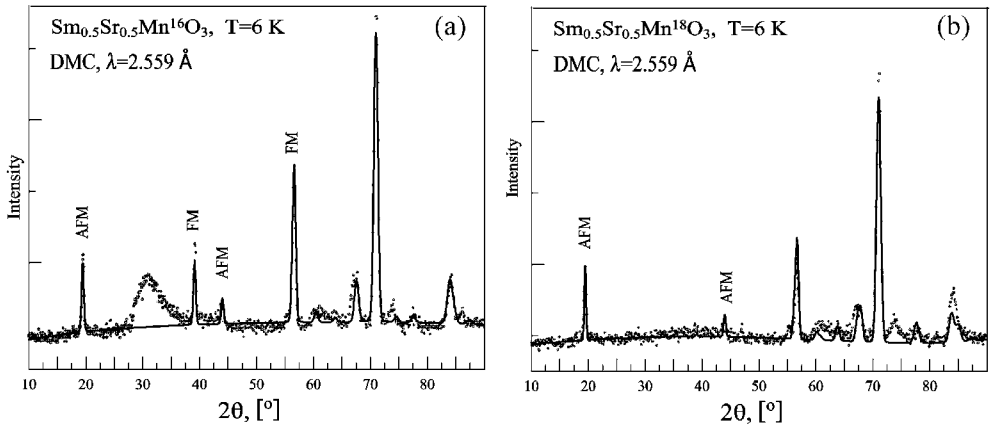

Figure 3. Neutron diffraction patterns of $^{152}Sm_{0.5}Sr_{0.5}MnO_3$ samples with ^{16}O (a) and ^{18}O (b). The most intense AFM and FM peaks are indicated. The broad peak in the SSM–^{16}O pattern originates from the sample environment.

studies dealt with the $x = 0.400$ composition [12, 13]. The neutron powder diffraction combined with the measurements of the second harmonic in the magnetic susceptibility and the low angle polarized neutron scattering provide an indication, in particular, of the existence of FM clusters with dimensions larger than 1000 Å in the paramagnetic matrix above the Curie temperature T_C. Below $T_C \approx 110$–120 K three magnetic phases—FM, AFM_A and AFM_{CE}—coexist, similarly to the case for the Nd–Sr system. In [18], the SSM-45 composition was investigated by means of neutron diffraction at several particular temperatures. In [18], the main attention is focused on the paramagnetic phase where the FM clusters with the characteristic size of about 8 Å are observed. These clusters are embedded into the orbitally and charge ordered (but without long range order) insulating matrix. Low temperature results suggest the existence of only FM ordering with $\mu_{FM} \approx 3.4\ \mu_B$.

The following detailed neutron diffraction experiments with $^{152}Sm_{0.55}Sr_{0.45}Mn^{16}O_3$, $^{152}Sm_{0.55}Sr_{0.45}Mn^{18}O_3$ and $^{152}Sm_{0.5}Sr_{0.5}Mn^{16}O_3$, $^{152}Sm_{0.5}Sr_{0.5}Mn^{18}O_3$ demonstrated a good agreement with the aforementioned data on the temperature dependence of the resistivity and magnetic susceptibility and, furthermore, these studies allowed us to determine unambiguously the types of magnetic ordering and their evolution with temperature. For SSM-45–^{16}O, the existence of only FM phase ($T_C \approx 120$ K, $\mu_{FM} = 3.24\ \mu_B$) was established, while in SSM-45–^{18}O an inhomogeneous state, FM + AFM_A ($\mu_{FM} = 0.8\ \mu_B$, $\mu_{AFM} = 1.7\ \mu_B$), was found below 100 K. Vice versa, the SSM-50–^{16}O was found in a mixed FM ($\mu_{FM} = 2.8\ \mu_B$) and AFM_A ($\mu_{AFM} = 1.9\ \mu_B$) state with dominant FM phase, whereas the ground magnetic state for the SSM-50–^{18}O sample is purely A-type antiferromagnetic ($\mu_{AF} = 1.7\ \mu_B$), as illustrated in figure 3. The reduced ordered magnetic moment in SSM-50–^{18}O is an indication that the AFM phase fills only a part of the sample volume. The mean ordered magnetic moment at the Mn ion in SSM-50–^{16}O ($\mu_{Mn} = (\mu_{FM}^2 + \mu_{AFM}^2)^{1/2}$) is equal to 3.4 μ_B. This value is very close to the expected mean value, calculated under the assumption that the structure contains 50% Mn^{3+} ($\mu = 4\ \mu_B$) and 50% Mn^{4+} ($\mu = 3\ \mu_B$). Assuming that the magnetic moments of the Mn ions are the same in the FM and AFM phases, one can find that these phases occupy approximately 68% and 32% of the sample volume, respectively.

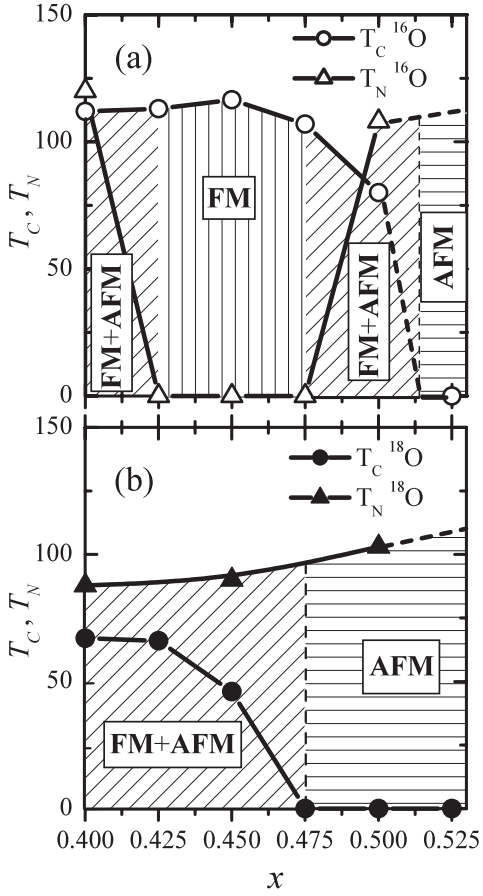

Figure 4. Phase diagram for $Sm_{1-x}Sr_xMnO_3$ with ^{16}O (a) and ^{18}O (b): the region with vertical hatching corresponds to the FM phase in ^{16}O samples; the region with horizontal hatching is the region of the AFM phase in ^{16}O and ^{18}O samples; the region with diagonal hatching is the phase separation region (FM + AFM) in ^{16}O and ^{18}O samples.

5. Phase diagram

On the basis of the whole set of our results, we are able to draw and compare the phase diagrams of $Sm_{1-x}Sr_xMnO_3$ with both oxygen isotopes (see figure 4). The special feature of the SSM-x–^{16}O phase diagram is the existence a narrow band ($0.425 \leqslant x \leqslant 0.475$) with a FM–M state between phase separated regions with FM–M and AFM_A phases. The prerequisite for such behaviour can be found in the phase diagram for $Ln_{0.5}Sr_{0.5}MnO_3$ system [19], where the temperature of transition into magnetically ordered state as a function of $\langle r_A \rangle$ is shown. The same type of phase diagram as for SSM-x–^{16}O was found for $Nd_{1-x}Sr_xMnO_3$ (see, for example, [20]) but with a much wider FM region.

The comparison of the changes in SSM-x phase diagrams due to the oxygen isotope substitution (^{16}O by ^{18}O) shows that they are first of all related to the suppression of stability for the ferromagnetic metallic state: (1) the isotope substitution is accompanied by the appreciable lowering of the Curie temperatures for all compositions; (2) a narrow region of existence for the homogeneous ferromagnetic state disappears; (3) the AFM ordering is observed now for

Table 1. Characteristic parameters of the compounds under study.

Composition	σ^2 (Å^2)	T_C (K)	ρ_{max} (Ω cm)
$Sm_{0.55}Sr_{0.45}MnO_3$	7.85×10^{-3}	126	65
$(NdEu)_{0.55}Sr_{0.45}MnO_3$	8.05×10^{-3}	114	111
$(NdTb)_{0.55}Sr_{0.45}MnO_3$	8.48×10^{-3}	80	5520

all compositions under study. The isotope effect in the concentration region under study is evidently asymmetric: the suppression of the ferromagnetic state is most clearly pronounced close to $x = 0.5$, while near $x = 0.4$ it is much weaker.

Note that in the parent $LaMnO_3$ compound, the AFM A-type ordering corresponds to the $d(3x^2 - r^2)/d(3y^2 - r^2)$ type of orbital ordering. With increasing doping level up to $x \approx 0.5$, the AFM_{CE} state with checkerboard charge ordering and the same $d(3x^2 - r^2)/d(3y^2 - r^2)$ type of ordering of Mn^{3+} e_g orbitals appears. However, it is most probable that in the SSM-x insulating phase close to $x = 0.5$, we have A-type antiferromagnetism with $d(x^2 - y^2)$-type orbital ordering, which is also compatible with checkerboard charge ordering [9, 21–23]. In this sense, SSM-x differs drastically from the $(La_{1-y}Pr_y)_{0.7}Ca_{0.3}MnO_3$ compound, which exhibits a metal–insulator transition induced by oxygen isotope substitution, but with the formation of an AFM_{CE} state. Thus, the manifestations of the isotope effect in manganites seem to be not closely related to the macroscopic features of their insulating state.

6. (Nd/Tb) and (Eu/Tb) compositions

To refine the specific role of Sm in producing unusual physical properties of SSM-x compounds, we also studied $(Nd_{1-y}Tb_y)_{0.55}Sr_{0.45}MnO_3$ and $(Eu_{1-y}Tb_y)_{0.55}Sr_{0.45}MnO_3$ manganites, where the relative content of rare earths Nd/Tb and Nd/Eu was chosen for retaining the same $\langle r_A \rangle$ values as in $Sm_{0.55}Sr_{0.45}MnO_3$. At the same time, the effect of local disorder due to size differences between A cations is characterized by the parameter $\sigma^2 = x_i r_i^2 - \langle r \rangle^2$, where x_i is the fractional occupancy of A site cations and r_i is the corresponding ionic radius. σ^2 has a pronounced effect on the macroscopic properties of these manganites (table 1).

Neutron diffraction study of the Nd/Tb–Sr demonstrated that in this compound as in SSM-45, magnetic moments of Mn are ordered ferromagnetically, but additionally there exists an ordering of magnetic moments of the rare earth cations below $T \approx 80$ K (see details in [16]).

For both Nd/Tb and Nd/Eu compounds, we performed measurements of the electrical resistivity $\rho(T)$ and magnetic susceptibility $\chi(T)$ and compared them with the results of the corresponding measurements for $Sm_{0.55}Sr_{0.45}MnO_3$. We also studied the effect of oxygen isotope substitution ($^{16}O \rightarrow {}^{18}O$) on these properties. In figures 5(a) and (b), we present the temperature dependence of the electrical resistivity for the Nd/Tb–Sr, Nd/Eu–Sr and Sm–Sr samples with ^{16}O and ^{18}O.

For the samples annealed in ^{16}O, the ρ values increase with σ, ρ_{max} increases by two orders of magnitude and the value of the temperature T_{MI} corresponding to the peak in resistivity (ρ_{max}) is shifted to lower temperatures (see the inset in figure 5(b)). The $(Nd/Eu)_{0.55}Sr_{0.45}MnO_3$ and $Sm_{0.55}Sr_{0.45}MnO_3$ samples annealed in ^{18}O remain metallic, whereas $(Nd/Tb)_{0.55}Sr_{0.45}MnO_3$ transforms to the insulating state, i.e. the latter sample undergoes a metal–insulator transition induced by the $^{16}O \rightarrow {}^{18}O$ isotope substitution.

In figures 6(a) and (b), we present the temperature dependence of the magnetic susceptibility for the same samples with ^{16}O and ^{18}O. In figure 6(a), we can see that for the samples with ^{16}O, the value of the magnetic susceptibility decreases and thus the content

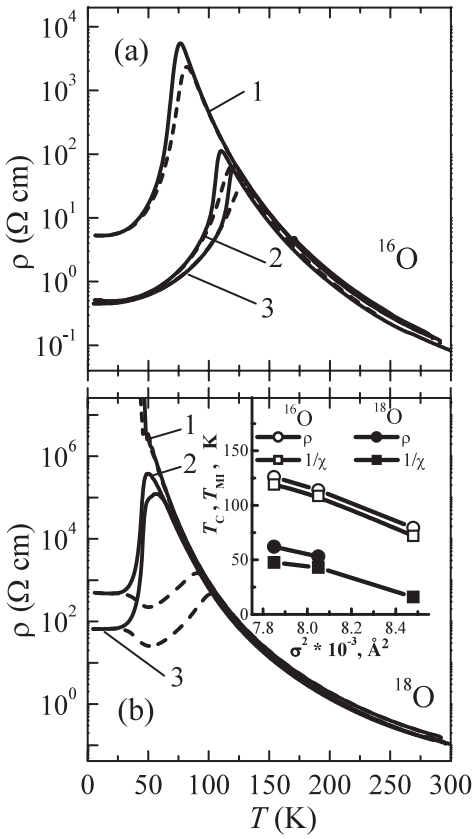

Figure 5. Temperature dependence of the electrical resistivity for $(NdTb)_{0.55}Sr_{0.45}MnO_3$ (1), $(NdEu)_{0.55}Sr_{0.45}MnO_3$ (2) and $Sm_{0.55}Sr_{0.45}MnO_3$ (3). The results for samples with ^{16}O and ^{18}O are presented in panels (a) and (b), respectively. Solid and dashed curves correspond to cooling and heating, respectively. The inset in panel (b) shows the T_C and T_{MI} dependence of σ^2. T_{MI} is determined as a point corresponding to the maximum temperature derivative of $\rho(T)$ below the resistivity peak.

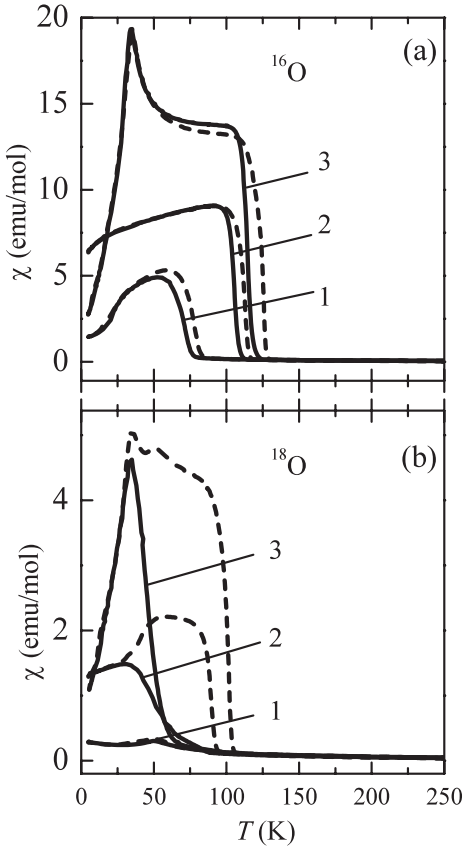

Figure 6. Temperature dependence of the ac magnetic susceptibility for $(NdTb)_{0.55}Sr_{0.45}MnO_3$ (1), $(NdEu)_{0.55}Sr_{0.45}MnO_3$ (2) and $Sm_{0.55}Sr_{0.45}MnO_3$ (3). The results for samples with ^{16}O and ^{18}O are presented in panels (a) and (b), respectively. Solid and dashed curves correspond to cooling and heating, respectively.

of FM phase decreases with increase in σ^2. The replacement of ^{16}O by ^{18}O leads to a much wider temperature hysteresis of the magnetic susceptibility, the volume content of FM phase significantly decreases and phase separation arises. In $(NdTb)_{0.55}Sr_{0.45}MnO_3$ sample with ^{18}O, the FM phase almost completely disappears. A more pronounced thermal hysteresis in $\rho(T)$ and $\chi(T)$ curves was observed for the samples with ^{18}O. It can be interpreted as a manifestation of their enhanced inhomogeneity and a broader range of phase separation. The relation between the degree of inhomogeneity and the width of the hysteresis was demonstrated by the comparison of neutron and susceptibility data for the LPCM-y system [24, 25]. Thus, the effect of $^{16}O \rightarrow {}^{18}O$ isotope substitution becomes more clearly pronounced with the growth of cation disorder in A positions. On the other hand, the absolute values of the susceptibility cannot be used directly to characterize the isotope effect because of the contribution of ordered magnetic moments of rare earth cations.

7. Conclusions

We found that the effect of $^{16}O \rightarrow {}^{18}O$ isotope substitution in complex manganese oxides is significantly enhanced near the crossover between different types of magnetic ordering, especially in the region corresponding to the formation of inhomogeneous states. This leads to a metal–insulator transition induced by the oxygen isotope substitution.

The effects of $^{16}O \rightarrow {}^{18}O$ isotope substitution in $R_{1-x}Sr_xMnO_3$ (R = Sm, Nd/Tb and Nd/Eu) manganites were analysed for two different cases:

(1) in $Sm_{1-x}Sr_xMnO_3$ compounds, the ground state was mainly affected by changing the cation doping level near $x = 0.5$, i.e. changing the relative content of Mn^{3+} and Mn^{4+} ions;
(2) in $R_{0.55}Sr_{0.45}MnO_3$, the cation disorder parameter σ^2 was changed by using Sm, (Nd/Tb) or (Nd/Eu) as the A cation.

We have shown that the oxygen isotope substitution in $R_{1-x}Sr_xMnO_3$ with x close to 0.5 leads to fundamental changes in the magnetic phase diagrams, which in general can be explained by the weakening of FM interactions. The region of the pure AFM insulating state enlarges; the pure FM–M state disappears, turning into a mixture of FM and AFM phases. A similar situation is found for the phase diagram of the LPCM-y compound with ^{16}O and ^{18}O isotopes [24]. The mechanisms of this isotope shift near the FM–AFM crossover were discussed in [26, 27]. The main idea is that the decrease in the amplitude of the zero vibrations for the heavier oxygen isotope causes a decrease in the effective electron hopping integral, thus favouring an insulating AFM phase near the FM–AFM crossover. Therefore, the oxygen isotope substitution shifts the energy balance between the metallic and insulating states and the metal–insulator transition can be interpreted as a percolation effect independent of the nature of the insulating phase.

Acknowledgments

The authors are grateful to A N Taldenkov for helpful assistance and for enlightening discussions. This work was supported by the Russian Foundation for Basic Research (projects 05-02-17600, 02-03-33258, 03-02-16954, 04-02-16991 and NSh-1694.2003.2).

References

[1] Uehara M, Mori S, Chen C H and Cheong S-W 1999 *Nature* **399** 560
[2] Cox D E, Radaelli P G, Marezio M and Cheong S-W 1998 *Phys. Rev.* B **57** 3305
[3] Balagurov A M, Pomjakushin V Yu, Sheptyakov D V, Aksenov V L, Gorbenko O Yu, Kaul A R and Babushkina N A 2001 *Phys. Rev.* B **64** 024420
[4] Nagaev E L 2001 *Phys. Rep.* **346** 388
[5] Dagotto E, Hotta T and Moreo A 2001 *Phys. Rep.* **344** 1
[6] Kagan M Yu and Kugel K I 2001 *Usp. Fiz. Nauk* **171** 577
Kagan M Yu and Kugel K I 2001 *Phys.—Usp.* **44** 553 (Engl. Transl.)
[7] Babushkina N A, Belova L M, Gorbenko O Yu, Kaul A R, Bosak A A, Ozhogin V I and Kugel K I 1998 *Nature* **391** 159
[8] Balagurov A M, Pomjakushin V Yu, Sheptyakov D V, Aksenov V L, Babushkina N A, Belova L M, Taldenkov A N, Inyushkin A V, Fischer P, Gutmann M, Keller L, Gorbenko O Yu and Kaul A R 1999 *Phys. Rev.* B **60** 383
[9] Kajimoto R, Yoshizawa H, Kawano H, Kuwahara H, Tokura Y, Ohoyama K and Ohashi M 1999 *Phys. Rev.* B **60** 9506
[10] Ritter C, Mahendiran R, Ibarra M R, Morellon L, Maignan A, Raveau B and Rao C N R 2000 *Phys. Rev.* B **61** R9229

[11] Martin C, Maignan A, Hervieu M and Raveau B 1999 *Phys. Rev.* B **60** 12191
[12] Runov V V, Chernyshov D Yu, Kurbakov A I, Runova M K, Trunov V A and Okorokov A I 2000 *Zh. Eksp. Teor. Fiz.* **118** 1174
Runov V V, Chernyshov D Yu, Kurbakov A I, Runova M K, Trunov V A and Okorokov A I 2000 *JETP* **91** 1017 (Engl. Transl.)
[13] Luzyanin I D, Ryzhov V A, Chernyshov D Yu, Kurbakov A I, Trounov V A, Lazuta A V, Khavronin V P, Larionov I and Dunaevsky S M 2001 *Phys. Rev.* B **64** 094432
[14] Babushkina N A, Chistotina E A, Gorbenko O Yu, Kaul A R, Khomskii D I and Kugel K I 2003 *Phys. Rev.* B **67** 100410(R)
[15] Babushkina N A, Chistotina E A, Gorbenko O Yu, Kaul A R, Kugel K I, Kurbakov A I, Trunov V A and Andrè G 2004 *Fiz. Tverd. Tela* **46** 1821
Babushkina N A, Chistotina E A, Gorbenko O Yu, Kaul A R, Kugel K I, Kurbakov A I, Trunov V A and Andrè G 2004 *Phys. Solid State* **46** 1884 (Engl. Transl.)
[16] Kurbakov A I, Trounov V A, Balagurov A M, Pomjakushin V Yu, Sheptyakov D V, Gorbenko O Yu and Kaul A R 2004 *Fiz. Tverd. Tela* **46** 1650
Kurbakov A I, Trounov V A, Balagurov A M, Pomjakushin V Yu, Sheptyakov D V, Gorbenko O Yu and Kaul A R 2004 *Phys. Solid State* **46** 1704 (Engl. Transl.)
[17] Balagurov A M, Pomjakushin V Yu, Sheptyakov D V, Aksenov V L, Babushkina N A, Belova L M, Gorbenko O Yu and Kaul A R 2001 *Eur. Phys. J.* B **19** 215
[18] De Teresa J M, Ibarra M R, Algarabel P, Morellon L, Garcia-Landa B, Marquina C, Ritter C, Maignan A, Martin C, Raveau B, Kurbakov A and Trounov V 2001 *Phys. Rev.* B **65** 100403(R)
[19] Woodward P M, Vogt T, Cox D E, Arulraj A, Rao C N R, Karen P and Cheetham A K 1998 *Chem. Mater.* **10** 3652
[20] Okuda T, Kimura T, Kuwahara H, Tomioka Y, Asamitsu A, Okimoto Y, Saitoh E and Tokura Y 1999 *Mater. Sci. Eng.* B **63** 163
[21] Mizokawa T and Fujimori A 1997 *Phys. Rev.* B **56** R493
[22] Maezono R, Ishihara S and Nagaosa N 1998 *Phys. Rev.* B **58** 11583
[23] van den Brink J and Khomskii D 1999 *Phys. Rev. Lett.* **82** 1016
[24] Balagurov A M, Pomjakushin V Yu, Sheptyakov D V, Babushkina N A, Gorbenko O Yu and Kaul A R 2004 *Physica* B **350** E1
[25] Babushkina N A, Belova L M, Taldenkov A N, Chistotina E A, Khomskii D I, Kugel K I, Gorbenko O Yu and Kaul A R 1999 *J. Phys.: Condens. Matter* **11** 5865
[26] Babushkina N A, Taldenkov A N, Belova L M, Chistotina E A, Gorbenko O Yu, Kaul A R, Kugel K I and Khomskii D I 1998 *J. Appl. Phys.* **83** 7369
[27] Plakida N M 2000 *Pis. Zh. Eksp. Teor. Fiz.* **71** 720
Plakida N M 2000 *JETP Lett.* **71** 493 (Engl. Transl.)